Biochimica et Biophysica Acta 1793 (2009) 1191–1198

Contents lists available at ScienceDirect

Biochimica et Biophysica Acta

journal homepage: www.elsevier.com/locate/bbamcr

Dynamic subcellular partitioning of the nucleolar transcription factor TIF-IA under ribotoxic stress

Jędrzej Szymański [a], Christine Mayer [b], Urs Hoffmann-Rohrer [b], Claudia Kalla [a], Ingrid Grummt [b], Matthias Weiss [a,*]

[a] Cellular Biophysics Group, German Cancer Research Center, D-69120 Heidelberg, Germany
[b] Division of Molecular Biology in the Cell II, German Cancer Research Center, DKFZ-ZMBH Alliance, D-69120 Heidelberg, Germany

ARTICLE INFO

Article history:
Received 3 November 2008
Received in revised form 9 April 2009
Accepted 11 May 2009
Available online 18 May 2009

Keywords:
Nucleolus
Ribotoxic stress
TIF-IA
Fluorescence recovery after photobleaching
Fluorescence correlation spectroscopy

ABSTRACT

TIF-IA is a basal transcription factor of RNA polymerase I (Pol I) that is a major target of the JNK2 signaling pathway in response to ribotoxic stress. Using advanced fluorescence microscopy and kinetic modeling we elucidated the subcellular localization of TIF-IA and its exchange dynamics between the nucleolus, nucleoplasm and cytoplasm upon ribotoxic stress. In steady state, the majority of (GFP-tagged) TIF-IA was in the cytoplasm and the nucleus, a minor portion (7%) localizing to the nucleoli. We observed a rapid shuttling of GFP-TIF-IA between the different cellular compartments with a mean residence time of ~130 s in the nucleus and only ~30 s in the nucleoli. The import rate from the cytoplasm to the nucleus was ~3-fold larger than the export rate, suggesting an importin/exportin-mediated transport rather than a passive diffusion. Upon ribotoxic stress, GFP-TIF-IA was released from the nucleoli with a half-time of ~24 min. Oxidative stress and inhibition of protein synthesis led to a relocation of GFP-TIF-IA with slower kinetics while osmotic stress had no effect. The observed relocation was much slower than the nucleo-cytoplasmic and nucleus–nucleolus exchange rates of GFP-TIF-IA, indicating a time-limiting step upstream of the JNK2 pathway. In support of this, time-course experiments on the activity of JNK2 revealed the activation of the JNK kinase as the rate-limiting step.

1. Introduction

The nucleolus is a sub-nuclear compartment in which ribosomal RNA synthesis and ribosome assembly take place. Apart from its traditional function as a ribosome factory, nucleoli have recently been shown to be also involved in viral replication, signal recognition, cell cycle regulation, and control of aging [1–3]. Related to their multiple duties, nucleoli show a strongly altered structure in many cancer types, a fact that might be connected to the intimate interplay of nucleolar proteins with the tumor suppressor p53 [4–6]. Contrary to the long-prevailing view, nucleolar proteins are not tightly bound to a nucleolar scaffold but rather show a very dynamic exchange with a free, nuclear pool [7–9]. Thus, the nucleolus is a dynamic entity that may rapidly integrate stimuli from upstream signaling cascades.

One type of signal that affects the nucleolar transcription machinery is the cellular response to stress [10]. Here, the cell aims at adapting to an unfavorable change in the environmental conditions, e.g. to cope with shortage of nutrients or exposure to oxidative stress. This response to extra- or intracellular stress involves drastic changes in gene expression. Stress stimuli have been shown to activate members of mitogen-activated protein kinases (MAPKs) and the c-Jun NH2-terminal protein kinases (JNKs). JNKs belong to stress-activated protein kinases (SAPKs) that play a pivotal role in the cellular response to environmental stress. Being stimulated by hyperosmotic shock, proinflammatory cytokines, or oxidative damage, they balance prosurvival stimuli with opposing proapoptotic signals. Anisomycin, a widely used inducer of SAPKs, inhibits eukaryotic peptidyl transferase, induces ribotoxic stress and activates JNKs which subsequently phosphorylate various target proteins, e.g. c-Jun, ATF-2, and Elk-1 [11].

The subcellular localization of regulatory factors is known to play a major role in the control of nuclear metabolism. Gene activation and assembly of the transcription machinery involves an orchestrated recruitment of chromatin remodeling complexes, transcription activators, transcription cofactors and the basal transcription machinery. Transcription of rRNA genes (rDNA) by RNA polymerase I (Pol I) is initiated by the step-wise assembly of a set of basal transcription factors, all of which are regulated by a complex set of post-translational modifications, such as phosphorylation, acetylation and others [12]. The key player in coordinating multiple signaling pathways is TIF-IA, a basal transcription initiation factor that is targeted by various protein kinases, including ERK, RSK [13], JNK2 [14], mTOR [15], and CK2 [16]. These kinases phosphorylate TIF-IA at multiple sites and phosphorylation controls the interaction with the TBP-containing factor TIF-IB/SL1 and/or with Pol I [16]. For example, ribotoxic stress that activates the c-Jun N-terminal kinase 2 (JNK2)

* Corresponding author. Tel.: +49 6221 5451304.
E-mail address: m.weiss@dkfz.de (M. Weiss).

0167-4889/$ – see front matter © 2009 Elsevier B.V. All rights reserved.
doi:10.1016/j.bbamcr.2009.05.004

leads to the phosphorylation of TIF-IA at a single threonine residue (Thr200) which in turn impairs the transcription complex formation and leads to the relocation of TIF-IA from the nucleolus to the nucleoplasm.

Here, we have used advanced fluorescence microscopy and kinetic modeling to describe and quantify the subcellular localization of TIF-IA and its exchange dynamics between individual cellular compartments upon ribotoxic, osmotic, or oxidative stress and after inhibiting protein synthesis. Our results show that in steady state the majority of the cellular TIF-IA protein pool is freely mobile in the cytoplasm and the nucleus (48% and 45%, respectively). Only a minor portion of TIF-IA (7%) localizes to the nucleoli. The local concentration of GFP-TIF-IA, however, was about 23-fold higher in the nucleolus and 3-fold higher in the nucleus than in the cytoplasm. Using fluorescence recovery after photobleaching (FRAP), we observed a rapid shuttling of GFP-TIF-IA between the respective compartments with a mean residence time of ~130 s in the nucleus and ~30 s in the nucleoli. The import rate from the cytoplasm to the nucleus was ~3-fold larger than the export rate suggesting the involvement of a nuclear import/export machinery rather than a passive diffusive transport. Upon application of ribotoxic stress via anisomycin treatment, GFP-TIF-IA was released from the nucleoli with a half-time of about 24 min, while the exchange between nucleus and cytoplasm was not affected. Oxidative stress and inhibition of protein synthesis led to a somewhat slower relocation (36–43 min half-time) while osmotic stress did not affect GFP-TIF-IA localization. In all cases, the observed relocation was very slow as compared to the nucleo-cytoplasmic and nucleus–nucleolus exchange rates of GFP-TIF-IA, the limiting factor being a rather slow activation of JNK2.

2. Materials and methods

2.1. Cell culture and transfection

We used a HeLa Flip-in stable cell line where expression of GFP-TIF-IA was controlled by a tetracycline regulated Tet-on system. Pol I reporter assays were performed as described previously [14]. Cells were kept in Dulbecco's modified Eagle Medium (DMEM) containing 10% Fetal Calf Serum (Doxycyclin free), 1% penicillin, 1 μg/ml Blasticidin, and 100 μg/ml Hygromycin. Blasticidin and Hygromycin were used as selection antibiotics for the expression of the GFP-TIF-IA plasmid. Anisomycin was dissolved in DMSO (stock solution 10 mM) and was added to live imaging medium (LIM) in a final concentration of 1 μM. For the control, the same amount of DMSO without anisomycin was added. Sodium arsenite (stock solution 1 M in water) was diluted in LIM to a final concentration of 100 μM; cycloheximide (stock solution 100 mg/ml in DMSO) was diluted in LIM to a final concentration of 10 μM; puromycin (stock solution 10 mM in water) was diluted in LIM to a final concentration of 10 μM; NaCl and sucrose were dissolved in LIM in a final concentration of 700 mM and 500 mM, repectively. Leptomycin B (stock solution 5.5 μg/ml in 70% MeOH/water) was dissolved in LIM to a final concentration of 1 ng/ml. Anisomycin, sodium arsenite, cycloheximide, puromycin, NaCl, sucrose and leptomycin B were purchased from Sigma-Aldrich.

2.2. Co-immunoprecipitation, immunoblotting and in vitro kinase assays

To analyze the interaction of TIF-IA with Pol I, cells overexpressing TIF-IA were lysed in IP buffer (20 mM Tris–HCl [pH 7.4], 200 mM NaCl, 2 mM EDTA, 2 mM EGTA, 1% Triton X-100), cleared by centrifugation at 10,000 ×*g* for 30 min, and the supernatants were incubated for 4 h at 4 °C with polyclonal anti-TIF-IA antibodies, pre-coupled to G-sepharose beads. The immunoprecipitates were washed with IP buffer containing 600 mM NaCl. Pol I was visualized on immunoblots with antibodies against the second largest subunit of Pol I (RPA116), TIF-IA with anti-TIF-IA antibodies. In vitro kinase activity of JNK was measured essentially as described in [14]. Briefly, HA-tagged JNK was purified from HEK293T cells overexpressing HA-JNK2. 5×10^6 cells were lysed in 0.8 ml IP buffer, centrifuged at 10,000 ×*g* for 20 min, and the supernatants were incubated for 4 h at 4 °C with 15 μg anti-HA antibodies bound to 20 μl protein G-agarose. Beads were washed 3 times with AM-400 and AM-100 and twice in 1.5× kinase buffer (37 mM Tris–HCl [pH 7.8], 10 mM $MgCl_2$, 1.5 mM DTT, 1.5 mM β-glycerophosphate, 0.1 mM Na_3VO_4). 1 μg GST-c-jun (1–166) was incubated in 15 μl kinase buffer containing 10 μCi [γ-^{32}P]ATP (5000 Ci/mmol) and 100 fmoles HA-JNK2. Phospho-GST-jun and immunoprecipitated HA-JNK2 were separated on 12% SDS-polyacrylamide gels and analyzed by autoradiograpy and immunoblotting using anti-HA antibodies, respectively.

2.3. Microscopy, FRAP, and FCS

Confocal imaging was performed with Leica SP2 and SP5 confocal microscopes (Leica Microsystems, Mannheim, Germany) using a 63×/1.4NA oil immersion objective. Samples were illuminated using the 488 nm line of an Argon laser and the fluorescence was detected with a 500–600 nm bandpass filter. Cells were imaged in LabTek chamber slides using phenol red-free live imaging medium supplemented with 4.5 g/l D-glucose, L-glutamine, and 25 mM HEPES, sodium pyruvate (1 mM) and Fetal Calf Serum (10%). Microscope and sample were kept at 37 °C by a climate chamber.

Time-lapse imaging after anisomycin treatment lasted for 3 h with a frame rate of 12/h or 6/h to decrease the effect of bleaching. Several cells (treated and control) were imaged in the same time course using the multipositioning tool of the microscope's software. At each position, a z-stack was acquired. The averaged decay curve for the nucleolar fluorescence was obtained from 10 different experiments.

In FRAP experiments, the nucleolus was bleached for 2–4 s and the nucleus for 6–10 s, decreasing the fluorescence to ~8% and ~20%, respectively. Data were fitted with a single exponential recovery curve (hence assuming the compartments to be well mixed [17]):

$$F(t) = A(1 - \exp(t/T)) + B$$

with $t_{1/2} = T\ln(2)$ the half-time of the recovery. The FRAP signal was corrected for a slight bleaching due to image acquisition by normalizing with respect to the total fluorescence of the entire cell at each time point. In all bleaching experiments we did not observe a significant immobile fraction.

FCS measurements were performed on a Leica SP2 with a water immersion objective (HCX PL APO 63× 1.2 W CORR) and an FCS-unit (Leica Microsystems, Mannheim, Germany). Samples were illuminated at 488 nm, the detection bandpass filter covered the range 500–530 nm; the pinhole was set to one Airy unit. Data were fitted using the fitting function for two non-interacting populations with normal diffusion [18]:

$$C(\tau) = \frac{fA}{\left(1+\tau/\tau_D^{(1)}\right)\times\sqrt{1+\tau/\left(S^2\tau_D^{(1)}\right)}} + \frac{(1-f)A}{\left(1+\tau/\tau_D^{(2)}\right)\times\sqrt{1+\tau/\left(S^2\tau_D^{(2)}\right)}}.$$

The prefactor A encodes (besides the photophysics of the GFP) the local concentration of the fluorescent TIF-IA as it is proportional to the inverse mean particle number in the focus. The first term with amplitude f describes a fast diffusing species, e.g. monomeric GFP-TIF-IA, while the second term with amplitude $(1-f)$ describes a slow-diffusing species, e.g. larger molecular complexes involving GFP-TIF-IA. For each cell an autocorrelation curve was collected for

60 s in the cytoplasm and the nucleus (count rate in the range 10–100 kHz). Higher concentrations, i.e. lower values for A, and slightly longer diffusion times τ_D[(1)] of GFP-TIF-IA were always observed in the nucleus compared to the cytoplasm (cf. Table 3).

The diffusion time in the above equation is connected to the size of the confocal volume, r_0, and the diffusion coefficient D of the fluorescent particle via $\tau_D = r_0^2/(4D)$. The diffusion coefficient on the other hand is determined via the Einstein–Stokes relations $D = k_B T/(6\pi\eta R)$ that depends on the thermal energy $k_B T$, the fluid's viscosity η, and the particle's radius R.

2.4. Image analysis

Image analysis and intensity determination were performed using ImageJ. Average intensities in the compartments were determined on single slices of z-stacks (taken with pinhole set to one Airy unit). The volume of each compartment (cytoplasm, nucleus, and nucleolus) was estimated using the Voxel Counter plugin of ImageJ on z-stacks. Relative volumes (averaged) were: cytoplasm 76%, nucleus 24%, and nucleolus 0.5%.

2.5. Modeling

To model and unify the exchange kinetics investigated by FRAP, we have formulated a simple three-state model using first-order kinetics (cf. Fig. 2B). The differential equations read:

$$\begin{aligned} \text{cytoplasm} \quad & \frac{dc}{dt} = \gamma n - rc \\ \text{nucleus} \quad & \frac{dn}{dt} = rc + \Gamma w - (R+\gamma)n \\ \text{nucleolus} \quad & \frac{dw}{dt} = Rn - \Gamma w \end{aligned} \tag{1}$$

where c, n, and w denote concentration of TIF-IA in cytoplasm, nucleus and nucleolus respectively. In steady state, the temporal derivatives on the left vanish, and one obtains for the steady-state fractions $\frac{n_0}{c_0} = \frac{r}{\gamma}$ and $\frac{w_0}{n_0} = \frac{R}{\Gamma}$. These fractions can be compared to the ratio of the steady-state average fluorescence in the respective compartments (cf. Table 1).

For simulating FRAP experiments, which involve total protein pools rather than concentrations, we needed to rewrite the above kinetic equations. Since the protein pool can be envisaged to be stationary (degradation and translation are slow on the time scale of the experiment) a particle conservation constraint $C+N+W = c\cdot V_C + n\cdot V_N + w\cdot V_W = 1$ applies to the above model (capital letters denote total protein pools in each compartment, i.e. $C = cV_C$, $N = nV_N$, and $W = wV_W$, where V stands for compartment volume). Using this constraint and assuming that volumes stay constant over time, the FRAP dynamics reads:

$$\begin{aligned} \text{cytoplasm} \quad & \frac{dC}{dt} = \gamma N/a - rC \\ \text{nucleus} \quad & \frac{dN}{dt} = -\left(\frac{dC}{dt} + \frac{dW}{dt}\right) \\ \text{nucleolus} \quad & \frac{dW}{dt} = RN/b - \Gamma W \\ \text{where } a = \frac{V_N}{V_C},\ & b = \frac{V_N}{V_W}. \end{aligned} \tag{2}$$

Simulating FRAP on the nucleus, the initial condition $(C,N,W) = (1,0,0)$ was chosen and Eq. (2) was integrated using a forward Euler scheme (time increment 1 s). Similarly, FRAP on the nucleolus was simulated by choosing $(C,N,W) = (0.37,0.53,0)/(0.37 \pm 0.53)$ as initial conditions (cf. Table 1). In these simulations, the rates γ and Γ were varied to best fit the experimental recovery curves while keeping the above determined ratios $\frac{n_0}{c_0} = \frac{r}{\gamma}$ and $\frac{n_0}{w_0} = \frac{\Gamma}{R}$ fixed. The full parameter set is shown in Table 2.

3. Results

3.1. Subcellular distribution of TIF-IA

To quantitatively assess the subcellular distribution of TIF-IA, we have generated HeLa/GFP-TIF-IA, a cell line that stably expresses GFP-tagged TIF-IA (GFP-TIF-IA) under the control of a tetracycline inducible promoter. The behavior of GFP-TIF-IA mimicked the behavior of endogenous TIF-IA, and cell morphology and proliferation were the same in uninduced and induced cells. To assay the activity of GFP-TIF-IA in Pol I transcription, we co-transfected GFP-TIF-IA with a Pol I reporter plasmid and monitored the level of reporter transcripts on Northern blots (Fig. 1). Similar to Flag-tagged TIF-IA that has been used in previous studies [10,13,14], GFP-TIF-IA stimulated Pol I transcription in a dose-dependent manner, demonstrating the functionality of GFP-tagged TIF-IA.

To quantify the subcellular distribution of GFP-TIF-IA, we utilized confocal images of HeLa/GFP-TIF-IA and monitored the fluorescence in the nucleolus, the nucleus, and the cytoplasm (see Fig. 2A for a representative example). First, we determined from a single confocal slice (~1 μm thickness) the local concentration of TIF-IA. To this end, we quantified the fraction of total fluorescence in each compartment (reflecting the number of GFP-TIF-IA molecules) and divided this number by the compartment's volume fraction (cf. highlighted boundaries in Fig. 2A). This analysis revealed that the concentration of TIF-IA is about 3-fold higher in the nucleus than in the cytoplasm while the nucleolus shows a 23-fold higher concentration of GFP-TIF-IA than the cytoplasm. These strong variations in the local concentration are also highlighted by a line-scan through the compartments in the fluorescence image (Fig. 2B).

To quantify the distribution of TIF-IA in the individual compartments, we determined the relative volumes of the compartments from a confocal z-stack and multiplied these by the previously determined concentrations. We found that 48% of total TIF-IA resides in the cytoplasm, 45% in the nucleoplasm, and 7% in the nucleoli. This result seems counterintuitive at first glance since the nucleolus appeared as the brightest cellular structure (cf. Fig. 2A, B). Yet, the prominent fluorescence highlights the high local concentration of GFP-TIF-IA in the nucleolus, while the hazy distribution of even larger amounts of nuclear or cytoplasmic TIF-IA molecules yields a dimmer fluorescence. These data are summarized in Table 1.

To get more insights from these experimental data, we have formulated a simple three-compartment model (see Fig. 2C and Materials and methods) in which TIF-IA is assumed to exchange between cellular compartments via a simple first-order kinetics. We have denoted by c, n, and w the protein concentrations in the cytoplasm, nucleus, and nucleolus, respectively. The import rate into the nucleus (from the cytoplasm) is denoted by r while the reverse transport happens with rate γ. Attachment and detachment at the nucleolus are denoted by the rates R and Γ. In steady state, the ratio of the cytoplasmic and the nuclear concentrations (n/c) are given by the ratio $r/\gamma \approx 2.9$, while the ratio of the nucleolar and the nuclear concentrations (w/n) is given by $R/\Gamma = 23.1/2.9 \approx 8$ (Table 1). While these ratios do not yet allow one to deduce the time scale of exchange between the compartments, another valuable information can already be derived at this point. We note that the exchange of TIF-IA between the nucleus and the cytoplasm is solely determined by the rates r and γ. If TIF-IA would enter and leave the nucleus by passive and undirected diffusion (similar to soluble GFP [19]) the ratio r/γ would have to be near to unity. The observed ratio $r/\gamma \approx 2.9$ highlights that the import into the nucleus is strongly favored, probably because the Ran/Importin machinery dominates over the counteracting export mechanism(s). Thus, transport between the nucleus and the

Table 1
Steady state distribution of GFP-TIF-IA as determined by image analysis of 16 cells and average FRAP recovery time ($n=18$ for nucleolus, $n=20$ for nucleus).

	Confocal slice			z-stack		FRAP $t_{1/2}$
	Volume fraction	Fluorescence fraction	Conc. w.r.t cytoplasm	Volume fraction	Fraction of total protein pool	
Cytoplasm	65.3% ± 6%	37% ± 8%	1	76%	48%	NA
Nucleus	33.9% ± 6%	53% ± 8%	2.9 ± 0.7	24%	45%	130 s ± 50 s
Nucleolus	0.8% ± 0.4%	10% ± 5%	23.1 ± 11.6	0.5%	7%	30 s ± 14 s

cytoplasm does not rely on passive diffusion but rather requires the importin/exportin machinery.

This hypothesis is further supported by noting that TIF-IA and GFP-TIF-IA have molecular weights of ~75 kDa and ~100 kDa, repectively, i.e. both are too large to cross the nuclear pore complex by simple diffusion [19]. Moreover, the amino-acid sequence of TIF-IA exhibits two regions that are homologous to a nuclear location signal (aa 568–572, KRSKK), and a nuclear export signal (aa 246–256, LIIEKLLKL) [20], respectively. Since we did not observe any change in the shuttling kinetics and subcellular distribution of GFP-TIF-IA upon application of leptomycin B, a potent inhibitor of exportin1-mediated export from the nucleus, we conclude that other exportins are responsible for the export of TIF-IA from the nucleus.

3.2. Shuttling kinetics of TIF-IA

To go beyond the steady-state picture and to determine the time scale needed for the exchange between the respective compartments, we have employed fluorescence recovery after photobleaching (FRAP). We first bleached the entire nucleus and monitored the recovery time (see Fig. 3A for a representative example). On average, the half-time for the recovery was $t_{1/2}\approx 130$ s, indicating a rapid shuttling of TIF-IA between the nucleus and the cytoplasm that is only 3–4-fold slower as compared to the passive diffusion of small molecules into the nucleus [19]. Thus, despite having a considerably higher mass than GFP alone, TIF-IA in complex with members of the import/export machinery can rapidly traverse the nuclear pores.

We next performed FRAP on the nucleolus (Fig. 3B) for which we obtained a typical recovery half-time of $t_{1/2}\approx 30$ s, demonstrating that on average TIF-IA resides for 30–40 s in the nucleolus. Thus, the exchange between the nucleolar and nuclear pool of TIF-IA is very rapid, therefore supporting a very dynamic steady state distribution of the protein that can quickly react on upstream signaling events. The recovery times are also summarized in Table 1.

Next, we used the kinetic model (cf. Fig. 2C and Materials and methods) to calculate in silico-FRAP curves for a large variety of parameter sets. By doing so, we aimed at identifying a unique parameter set that yields a best fit to the experimental results (steady-state values and FRAP curves, Table 1). By requiring a good fit to both sets of experimental FRAP data, we were indeed able to identify a unique parameter set, i.e. we could extract the import and export rates r, R, γ, and Γ individually (summarized in Table 2). Using these rates, we may predict the loss of TIF-IA from the nucleoli (see next section) by setting $R=\Gamma$, i.e. TIF-IA can enter and leave the nucleolus with equal probabilities. This model approach hence predicts a very fast decay of the nucleolar fluorescence (half-time $\tau_{1/2}=\ln 2/\Gamma\approx 33$ s) upon stressing cells with anisomycin or other JNK-activating substances.

Table 2
Rate constants of the model (cf. Fig. 2C) that yielded the best fit to the averaged experimental data.

R	r	Γ	γ
1.67×10^{-1}/s	3.3×10^{-3}/s	2.1×10^{-2}/s	1.15×10^{-3}/s

The import rate into the nucleus is increased with respect to the export rate, suggesting the involvement of the export/import machineries rather than diffusive transport. Similarly, the dominant association rate R explains the high local concentration of TIF-IA in the nucleoli.

3.3. Mobility of TIF-IA in the cytoplasm and the nucleus

To exclude a diffusion-limited binding of TIF-IA to the nucleolus (which we tacitly assumed in the above model) we used fluorescence correlation spectroscopy (FCS). This method not only allows measurements of the mobility of TIF-IA in the nucleus and the cytoplasm, but also of the local concentration of TIF-IA in these compartments (cf. Table 3). Fig. 4 shows representative FCS curves for both compartments. In all cases, the FCS curves were most consistent with the assumption of two GFP-TIF-IA pools that have different mobilities (see Materials and methods for details). The faster pool with a mean residence time $\tau_D{}^{(1)}$ in the confocal volume comprised the majority (~80%) of the total GFP-TIF-IA pool. The value for $\tau_D{}^{(1)}$ was 1.2-lower in the cytoplasm than in the nucleus (Table 3). The value $\tau_D{}^{(1)}\approx 560$ μs found for the fast cytoplasmic pool is indicative for a free diffusion of monomeric GFP-TIF-IA. Assuming a globular conformation of TIF-IA, one can deduce from the molecular weight a hydrodynamic radius of ~3.5 nm for GFP-TIF-IA. Inserting this into the Einstein–Stokes relation and assuming a roughly 4-fold higher cytoplasmic viscosity as compared to water [21], one obtains a diffusion coefficient $D\approx 15$ μm^2/s and thus a residence time $\tau_D{}^{(1)}\approx 670$ μs. This value is in good agreement with the experimentally determined value. The slightly larger value in the nucleus indicates that TIF-IA may form here a complex with other proteins, e.g. components of the transcription machinery. The low amount (~20%) of slow-diffusing GFP-TIF-IA most likely represents those molecules that interact with multiple components of the nuclear import/export machinery.

Although the determined mobility of GFP-TIF-IA was slightly different in the cytoplasm and the nucleus, one can deduce from the typical residence time $\tau_D{}^{(1)}<1$ ms in the focus (which has a volume of less than 1 μm^3) that a TIF-IA molecule diffusively explores the entire nucleus within less than 1 s. Therefore, the diffusion is much faster than the exchange between the nucleus and nucleolus, or nucleus and cytoplasm. Hence one can regard the compartments as well mixed, i.e. diffusion-limited binding is negligible.

Using FCS, it is possible to determine the number N of fluorescent molecules in the confocal volume (cf. Materials and methods), i.e. to probe the local concentration of GFP-TIF-IA. In agreement with our image analysis data (Table 1), we observed a ratio of $n/c\approx 2.9$ between the nuclear and cytoplasmic concentrations. Notably, this ratio did not depend on the expression level of GFP-TIF-IA (Fig. 4B).

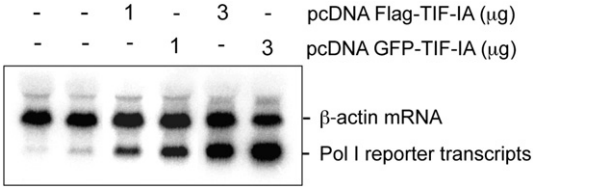

Fig. 1. GFP-tagged TIF-IA stimulates Pol I transcription. HEK293T cells were co-transfected with a human Pol I reporter plasmid and 1 and 3 μg of either pcDNA-Flag-TIF-IA or pcDNA-GFP-TIF-IA. Reporter transcripts and β-actin mRNA levels were monitored on Northern blots.

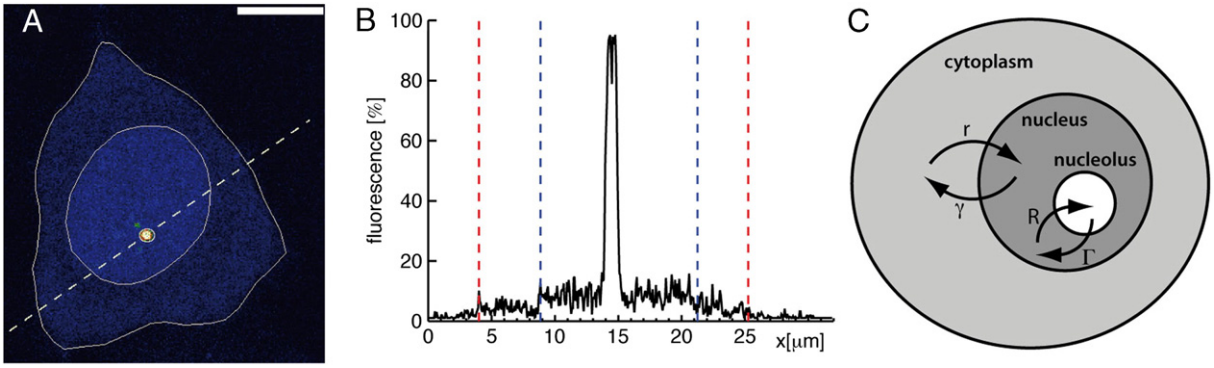

Fig. 2. Steady-state fluorescence of HeLa cells stably expressing GFP-TIF-IA. (A) Confocal fluorescence picture of HeLa/GFP-TIF-IA; compartment boundaries are highlighted by bright lines. The cytoplasm, nucleus, and nucleolus can be clearly distinguished. (B) The fluorescence intensity changes along the indicated line, highlighting the increasing concentration of GFP-TIF-IA from the cytoplasm to the nucleus and on to the nucleolus. Boundaries of cytoplasm and nucleus are highlighted in red and blue, respectively. (C) Three-compartment model for the kinetic shuttling of TIF-IA with indicated transport rates.

3.4. Release of TIF-IA from the nucleolus upon ribotoxic stress

We next monitored the loss of nucleolar fluorescence after treating cells with the ribotoxic agent anisomycin. Representative time courses of an untreated and an anisomycin-treated cell are shown in Fig. 5A. Nucleolar fluorescence decayed with a half-time of about 24 min, i.e., the kinetics was at 1–2 orders of magnitude slower than the exchange kinetics between the respective compartments. The loss of nucleolar fluorescence after anisomycin treatment is further highlighted by a more than 4-fold decrease in the ratio of nucleolar and nuclear concentrations of TIF-IA after 3 h (untreated $w/n \approx 8$; treated $w/n \approx 1.7$). Thus, upon exposure to ribotoxic stress, the concentration of nucleolar TIF-IA is similar to that of the nucleoplasm. In contrast, the relative concentrations of nuclear and cytoplasmic GFP-TIF-IA as measured by FCS and image analysis did not change after anisomycin treatment, indicating that nuclear import and export of TIF-IA were not affected by ribotoxic stress.

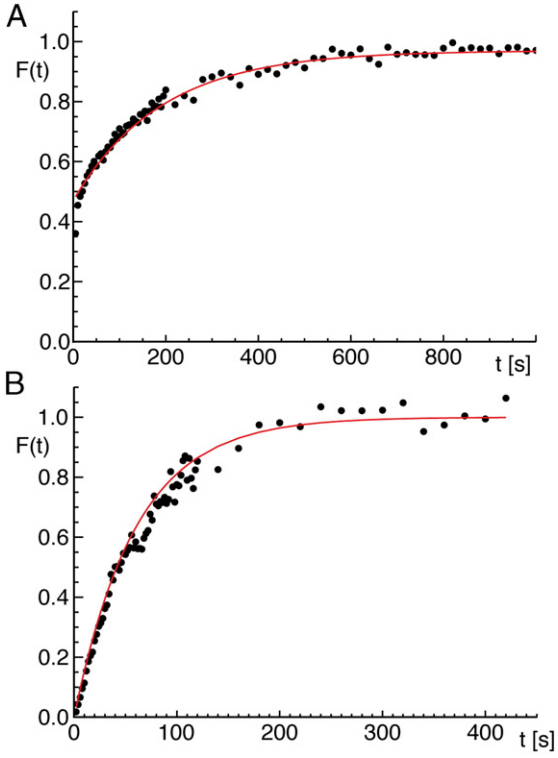

Fig. 3. Shuttling kinetics of TIF-IA between compartments as seen by FRAP. (A) After photobleaching the entire nucleus the fluorescence recovers with a half-time of $t_{1/2} = 130\ s \pm 50\ s$. (B) The recovery time of nucleolar TIF-IA is $t_{1/2} = 30\ s \pm 14\ s$. Symbols are data from a single cell, full lines are recovery curves from the model (parameters are listed in Table 2).

The slow decay of the nucleolar fluorescence (~24 min) in anisomycin-treated cells is inconsistent with the estimated ~33 s derived from our simple kinetic model and the steady-state exchange rates (Table 2). Indeed, as anisomycin-induced phosphorylation of TIF-IA should impair transcription complex formation [14], even a slightly shorter time would be expected because of an increased off-rate Γ. This discrepancy to the experimental data indicates that the dominant time scale of the relocation of TIF-IA is not governed by the steady-state exchange rates depicted in the model, but rather that another process must set the limiting steps.

In order to determine the order of events in the upstream signaling cascade, we performed time-course experiments analyzing JNK2 activation. We also followed transcription complex integrity upon anisomycin treatment. Consistent with earlier reports [22], JNK activity is induced after approximately 30 min (Fig. 6A), demonstrating a window of activation between 20 and 30 min in most human cell lines. Concomitantly, TIF-IA was released from Pol I within the same time frame, as shown by co-immunoprecipitation experiments (Fig. 6B). Thus, the major limitation in the cascade is the activation of the JNK kinase, followed by a fast phosphorylation of TIF-IA, which is, subsequently, slowly released from the nucleoli.

3.5. Localization of TIF-IA under various forms of stress

We next compared the dynamic relocation of TIF-IA from the nucleoli after ribotoxic stress to other forms of cellular stress that involve the JNK pathway. These data are summarized in Table 4. In particular, we applied osmotic and oxidative stresses. While applying osmotic stress did not induce a change in GFP-TIF-IA localization within 3 h, oxidative stress caused a loss of GFP-TIF-IA from the nucleoli with a half-time of 36 min. Being significantly slower than the reaction upon ribotoxic stress, yet still being in the same order of magnitude, this result highlights that JNK-triggered stress response may be activated along different routes with different kinetics. Indeed, ribotoxic and oxidative stresses have been shown earlier to activate the JNK pathway via different routes [23]. The somewhat faster

Table 3
FCS data on GFP-TIF-IA averaged over ~100 measurements in 50 different cells.

	N	$\tau_D^{(1)}$	Fraction f	$\tau_D^{(2)}$
Cytoplasm	4.2	559 μs	76%	10 ms
Nucleus	12.1	680 μs	72%	15 ms

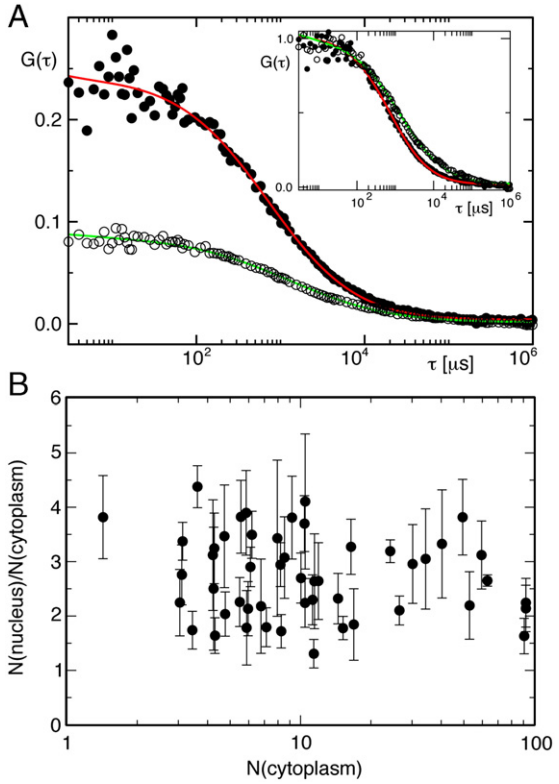

Fig. 4. Mobility of TIF-IA in the cytoplasm and the nucleus. (A) Representative FCS curves for the diffusion of GFP-TIF-IA in the cytoplasm (full black circles) and the nucleus (open circles). Full lines are fits according to Eq. (2). The lower amplitude for the nucleus highlights the higher concentration of GFP-TIF-IA in the nucleus as compared to the cytoplasm. Inset: Normalizing both curves highlights the faster decay of the cytoplasmic curve (filled symbols), i.e. a lower value of $\tau_D^{(1)}$ (Table 3). (B) The ratio of concentrations of GFP-TIF-IA in the nucleus and cytoplasm (n/c), as determined from the offsets of the FCS curves for a cell population does not depend on the expression level of GFP-TIF-IA as quantified via the average number of GFP-TIF-IA proteins in the focus (N) when measuring in the cytoplasm. The average ratio is $n/c = 2.9 \pm 0.7$. Error bars were estimated from three measurements in the cytoplasm and nucleus per cell.

relocation of TIF-IA in response to ribotoxic stress may hence reflect the somewhat faster signal transduction of one of these routes.

Blocking protein synthesis also induced a relocation of GFP-TIF-IA (half-time 36–43 min). Indeed, JNKs have, in part, been identified as signaling molecules that become active in response to the application of cycloheximide, a potent inhibitor of protein synthesis [24]. Hence, also this particular form of cellular stress leads to a JNK-triggered relocation of TIF-IA with a kinetics similar to that observed for oxidative stress.

4. Discussion

Signaling processes in a living cell are highly dynamic events that require an orchestrated and coordinated reaction of many proteins and signaling molecules. Triggering, for example, stress-activated protein kinases, results in a phosphorylation of the nucleolar transcription factor TIF-IA and its subsequent loss from the nucleolus, hence shutting down the production of ribosomal RNA. Here, we have studied the exchange of TIF-IA between the cytoplasm, the nucleus, and the nucleolus, its diffusion in these compartments, and the time course of the reaction after applying various stress factors to the cell. We have found that TIF-IA is a highly dynamic transcription factor that rapidly shuttles between the compartments. Indeed, GFP-TIF-IA, having a mass of ~100 kDa, traveled from the cytoplasm to the nucleus within 2–3 min. Taking into account a molecular cut-off of ~40 kDa for passive diffusion through the nuclear pore complex [19] the import and export most likely depend on the importin/exportin machinery. Since we did not observe any sensitivity to leptomycin B, other exportins than exportin1 can be expected to facilitate exit from the nucleus. Using a simple three-compartment model, we were also able to determine the import vs. the export rate, indicating that the import rate is ~3 times larger than the export rate. Assuming a cellular volume of 1–10 nl and an overall concentration of TIF-IA of 10–100 nM, the determined import rate translates into 10^4–10^6 proteins that are exchanged between nucleus and cytoplasm every second.

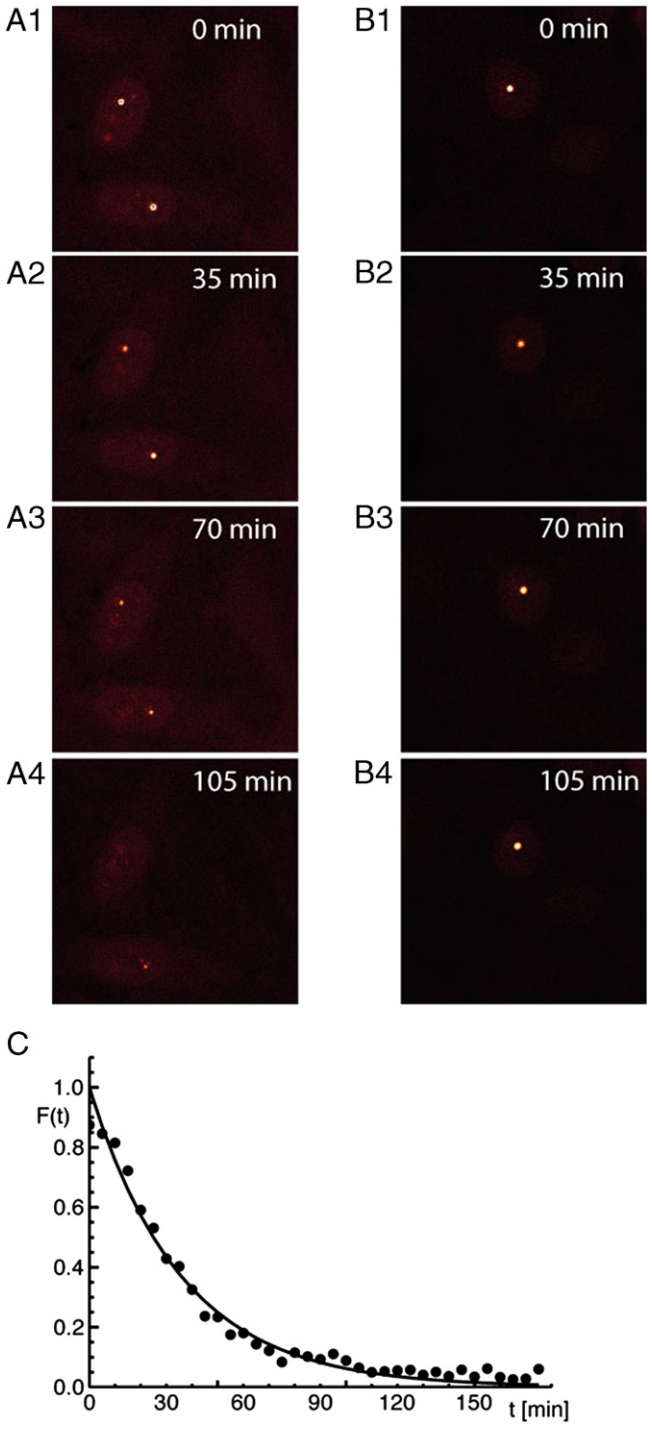

Fig. 5. Response of TIF-IA to ribotoxic stress. (A1–A4) Decay of the nucleolar localization of GFP-TIF-IA after anisomycin treatment. (B1–B4) Control cells kept their phenotype. (C) The averaged loss of nucleolar fluorescence to background levels had a half-time of ~24 min, i.e. it was much slower than the shuttling kinetics between the compartments.

A large free pool of TIF-IA molecules (only ~7% of the protein was located on average in the nucleolus) was available in the cytoplasm and the nucleus, which may facilitate a fast response of TIF-IA to changes in the environmental conditions via upstream signaling cascades. Yet, the observed reaction time after applying ribotoxic stress via anisomycin was much slower than expected from the rapid shuttling kinetics of TIF-IA. From our data, one major bottleneck in the signaling cascade appears to be the slow activation of the upstream protein kinase JNK which is consistent with earlier reports, demonstrating a peak activity 20–30 min after anisomycin in most human cell lines [22]. This is followed by a very quick phosphorylation of TIF-IA and dissociation from the transcription complex. The final step is the release from the nucleoli.

TIF-IA was relocated from the nucleoli upon application of ribotoxic stress (anisomycin), oxidative stress (sodium arsenite), and translational inhibitors (cycloheximide, puromycin), but not after osmotic stress. It has been reported that anisomycin is a strong agonist of SAPK/JNK (20-fold activation), while the other drugs activate JNKs only up to 4–5 folds [11]. One could argue that either the mild activation is sufficient for the shuttling response — or alternatively, it is possible that there is a direct link between translational output and TIF-IA localization in addition to JNK activity. The latter possibility could for instance, involve proteins from the 14-3-3 family which are known to communicate between kinases, such as the ribosomal S6 kinase p90 and target proteins in the nucleus/nucleolus [25].

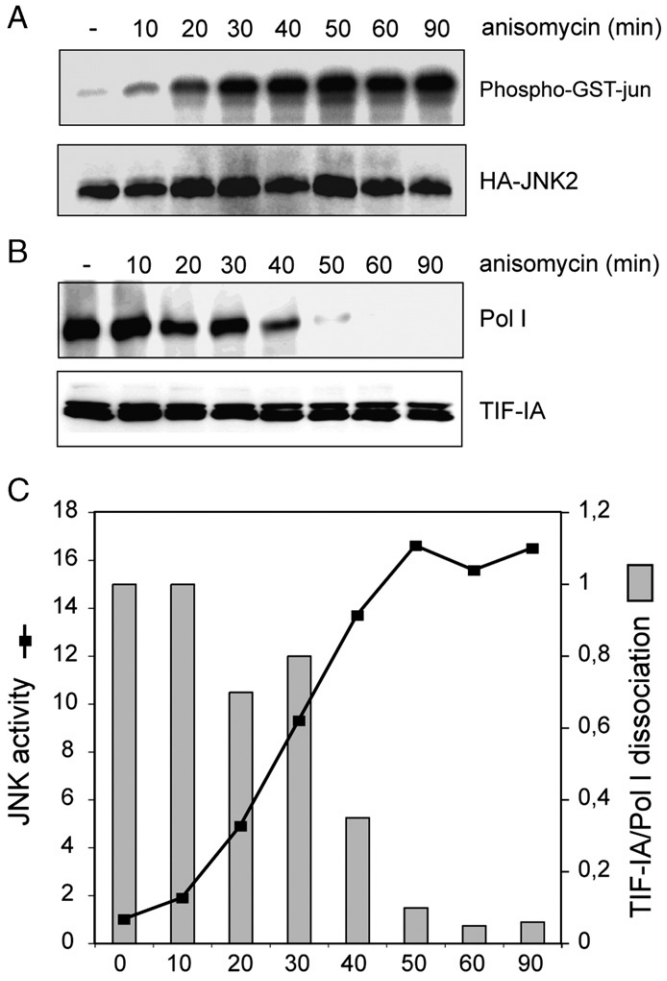

Fig. 6. Time course of JNK activation and transcription complex integrity upon anisomycin treatment. (A) To measure JNK2 activity, cells were transfected with pcDNA3.1HA-JNK2 and subjected to 1 μM anisomycin for the indicated times. HA-JNK2 was immunopurified from 10^6 cells and tested for kinase activity using purified GST-tagged c-Jun (aa 1–166). Western blots of cellular lysates were probed using antibodies against overexpressed HA-JNK2. (B) Interaction of TIF-IA and Pol I was determined by immunoprecipitation of TIF-IA. TIF-IA and co-precipitated Pol I were visualized on Western blots using α-TIF-IA and α-RPA116 antibodies, respectively. (C) Diagram showing the quantification of phospho-c-Jun (normalized to HA-JNK Western blot units, dark lines) and TIF-IA/Pol I interaction (gray bars). Error bars denote the standard deviation derived from two independent experiments.

Table 4
Summary of TIF-IA loss kinetics after application of stress.

Stress type	Substance	Concentration	Decay half-time [min]
Ribotoxic	Anisomycin	1 μM	24
Oxidative	Sodium arsenite	100 μM	36
Osmotic	NaCl	700 mM	No decay within 3 h
	Sucrose	500 mM	No decay within 3 h
Inhibition of protein synthesis	Cyclohexamide	10 μM	36
	Puromycin	1 μM	43

Acknowledgements

This work was supported by the Institute for Modeling and Simulation in the Biosciences (BIOMS) in Heidelberg. JS received funding from the Initiative and Networking Fund of the Helmholtz Association within the Helmholtz Alliance on Systems Biology.

References

[1] F.M. Boisvert, S. van Koningsbruggen, J. Navascues, A.I. Lamond, The multifunctional nucleolus, Nat. Rev. 8 (2007) 574–585.
[2] B.K. Dove, J.H. You, M.L. Reed, S.R. Emmett, G. Brooks, J.A. Hiscox, Changes in nucleolar morphology and proteins during infection with the coronavirus infectious bronchitis virus, Cell. Microbiol. 8 (2006) 1147–1157.
[3] R. Visintin, A. Amon, The nucleolus: the magician's hat for cell cycle tricks, Curr. Opin. Cell Biol. 12 (2000) 372–377.
[4] D.M. Gilkes, J. Chen, Distinct roles of MDMX in the regulation of p53 response to ribosomal stress, Cell Cycle (Georgetown, Tex) 6 (2007) 151–155.
[5] R.J. White, RNA polymerases I and III, growth control and cancer, Nat. Rev. 6 (2005) 69–78.
[6] X. Yuan, Y. Zhou, E. Casanova, M. Chai, E. Kiss, H.J. Grone, G. Schutz, I. Grummt, Genetic inactivation of the transcription factor TIF-IA leads to nucleolar disruption, cell cycle arrest, and p53-mediated apoptosis, Mol. Cell 19 (2005) 77–87.
[7] M. Dundr, U. Hoffmann-Rohrer, Q. Hu, I. Grummt, L.I. Rothblum, R.D. Phair, T. Misteli, A kinetic framework for a mammalian RNA polymerase in vivo, Science (New York, N.Y) 298 (2002) 1623–1626.
[8] S.A. Gorski, S.K. Snyder, S. John, I. Grummt, T. Misteli, Modulation of RNA polymerase assembly dynamics in transcriptional regulation, Mol. Cell 30 (2008) 486–497.
[9] Y.W. Lam, A.I. Lamond, M. Mann, J.S. Andersen, Analysis of nucleolar protein dynamics reveals the nuclear degradation of ribosomal proteins, Curr. Biol. 17 (2007) 749–760.
[10] C. Mayer, I. Grummt, Cellular stress and nucleolar function, Cell Cycle (Georgetown, Tex) 4 (2005) 1036–1038.
[11] M.S. Iordanov, D. Pribnow, J.L. Magun, T.H. Dinh, J.A. Pearson, S.L. Chen, B.E. Magun, Ribotoxic stress response: activation of the stress-activated protein kinase JNK1 by inhibitors of the peptidyl transferase reaction and by sequence-specific RNA damage to the alpha-sarcin/ricin loop in the 28S rRNA, Mol. Cell. Biol. 17 (1997) 3373–3381.
[12] I. Grummt, Life on a planet of its own: regulation of RNA polymerase I transcription in the nucleolus, Genes Dev. 17 (2003) 1691–1702.
[13] J. Zhao, X. Yuan, M. Frodin, I. Grummt, ERK-dependent phosphorylation of the transcription initiation factor TIF-IA is required for RNA polymerase I transcription and cell growth, Mol. Cell 11 (2003) 405–413.
[14] C. Mayer, H. Bierhoff, I. Grummt, The nucleolus as a stress sensor: JNK2 inactivates the transcription factor TIF-IA and down-regulates rRNA synthesis, Genes Dev. 19 (2005) 933–941.
[15] C. Mayer, J. Zhao, X. Yuan, I. Grummt, mTOR-dependent activation of the transcription factor TIF-IA links rRNA synthesis to nutrient availability, Genes Dev. 18 (2004) 423–434.
[16] H. Bierhoff, M. Dundr, A.A. Michels, I. Grummt, Phosphorylation by casein kinase 2 facilitates rRNA gene transcription by promoting dissociation of TIF-IA from elongating RNA polymerase I, Mol. Cell. Biol. 28 (2008) 4988–4998.
[17] M. Weiss, Challenges and artifacts in quantitative photobleaching experiments, Traffic (Copenhagen, Denmark) 5 (2004) 662–671.
[18] P. Schwille, J. Bieschke, F. Oehlenschlager, Kinetic investigations by fluorescence correlation spectroscopy: the analytical and diagnostic potential of diffusion studies, Biophys. Chem. 66 (1997) 211–228.
[19] K. Ribbeck, D. Gorlich, Kinetic analysis of translocation through nuclear pore complexes, EMBO J. 20 (2001) 1320–1330.

[20] W. Wen, J.L. Meinkoth, R.Y. Tsien, S.S. Taylor, Identification of a signal for rapid export of proteins from the nucleus, Cell 82 (1995) 463–473.
[21] M. Elsner, H. Hashimoto, J.C. Simpson, D. Cassel, T. Nilsson, M. Weiss, Spatiotemporal dynamics of the COPI vesicle machinery, EMBO Rep. 4 (2003) 1000–1005.
[22] C.P. Bagowski, J. Besser, C.R. Frey, J.E. Ferrell Jr., The JNK cascade as a biochemical switch in mammalian cells: ultrasensitive and all-or-none responses, Curr. Biol. 13 (2003) 315–320.
[23] M.S. Iordanov, B.E. Magun, Different mechanisms of c-Jun NH(2)-terminal kinase-1 (JNK1) activation by ultraviolet-B radiation and by oxidative stressors, J. Biol. Chem. 274 (1999) 25801–25806.
[24] R.K. Barr, M.A. Bogoyevitch, The c-Jun N-terminal protein kinase family of mitogen-activated protein kinases (JNK MAPKs), Int. J. Biochem. Cell Biol. 33 (2001) 1047–1063.
[25] M.E. Cavet, S. Lehoux, B.C. Berk, 14-3-3beta is a p90 ribosomal S6 kinase (RSK) isoform 1-binding protein that negatively regulates RSK kinase activity, J. Biol. Chem. 278 (2003) 18376–18383.